CdSe nanoparticles dispersed in ferroelectric smectic liquid crystals: Effects upon the smectic order and the smectic-*A* to chiral smectic-*C* phase transition

Angelos Thanassoulas,[1] Eva Karatairi,[1] George Cordoyiannis,[2,3] Zdravko Kutnjak,[3,4] Vassilios Tzitzios,[1,5] Ioannis Lelidis,[2] and George Nounesis[1,*]

[1]*Biomolecular Physics Laboratory, National Centre for Scientific Research "Demokritos," 15310 Aghia Paraskevi, Greece*

[2]*Department of Physics, National and Kapodistrian University of Athens, 15784 Zografou, Greece*

[3]*Condensed Matter Physics Department, Jožef Stefan Institute, 1000 Ljubljana, Slovenia*

[4]*Center of Excellence NAMASTE, 1000 Ljubljana, Slovenia*

[5]*Institute of Materials Science, National Centre for Scientific Research "Demokritos," 15310 Aghia Paraskevi, Greece*

(Received 5 March 2013; published 18 September 2013)

Spherical CdSe nanoparticles, surface-treated with oleylamine and tri-octylphosphine, dispersed in ferroelectric liquid crystals, can efficiently target disclination lines, substantially altering the macroscopic properties of the host compound. Here we present an ac calorimetry and x-ray diffraction study demonstrating that for a large range of nanoparticle concentrations the smectic-*A* layer thickness increases monotonically. This provides evidence for enhanced accumulation of nanoparticles at the smectic layers. Our results for the Smectic-*A* (Sm*A*) to chiral smectic-*C* (SmC^*) phase transition of the liquid crystal S-(+)4-(2′-methylbutyl)phenyl-4′-n-octylbiphenyl-4-carboxylate (CE8) reveal that the character of the transition is profoundly changed as a function of the nanoparticle concentration. Large transition temperature shifts are recorded. Moreover, the heat-capacity peaks exhibit a crossover trend to a step-like anomaly. This behavior may be linked to the weakening of the Sm*A* and SmC^* order parameter coupling responsible for the observed near-tricritical, mean-field character of the transition in bulk CE8. At lower temperatures, the presence of nanoparticles disrupts the phase sequence involving the tilted hexatic phases most likely by obstructing the establishment of long-range bond-orientational order.

DOI: 10.1103/PhysRevE.88.032504 PACS number(s): 61.30.Jf, 81.07.Ta, 61.05.cp

I. INTRODUCTION

Liquid crystals (LCs) containing dispersed nanoparticles of various shapes and sizes hold a great promise for scientific advancement and technological breakthroughs in the display and sensor industries, for the development of nanoscaffolds and novel concepts for the design of liquid-crystalline metamaterials [1,2]. The coupling of the anisotropic elasticities of the liquid-crystalline medium to optical, conductive, or magnetic properties of the nanoparticles is expected to have a significant impact, extending the macroscopic properties of LC-mesophases to new extremes bearing direct consequences upon the relevant technologies [3–5]. On the other hand, the unraveling of the mechanisms driving the self-assembly of surface-functionalized nanoparticles in the liquid-crystalline environment will pave the way for developing bottom-up approaches for the construction of super-structures in the microscale with customized secondary and tertiary architecture [6]. This is undoubtedly one of the major challenges of nanotechnology today. It is thus imperative to control how surface-treated nanoparticles can interact with liquid crystals so that the macroscopic properties of the host can be tailored for specific applications while the nanoproperties of the dopants can be harvested for the design of novel hybrid materials.

From the point of view of phase transitions and critical phenomena, a large amount of the published work has involved dispersions of aerosils (hydrophillically or hydrophobically treated SiO_2 spherular particles with diameter $d \sim 7$ nm) in chiral and nonchiral thermotropic compounds, investigating the effects upon the isotropic to nematic (*I*-*N*), *N* to smectic-*A* (Sm*A*), Sm*A* to smectic-*C* (Sm*C*), and Sm*A* to chiral smectic-*C* (SmC^*) transitions [7–19]. It has been demonstrated by several studies that aerosils dispersed in LCs lead to the destruction of the quasilong range smectic order even at the very low aerosil concentrations [8]. Aerosils tend to organize in adaptive, randomly connected networks and are thus displaying universal properties, including their characteristic response to external stresses, undergoing a soft-stiff-regime type of transformation as a function of the nanoparticle concentration [7,20]. In the stiff regime, the entrapment of liquid crystal molecules in nanoparticle-formed cavities with rigid walls in all possible orientations, imposes a quenched random disorder field upon the liquid-crystalline ordering.

In general, dispersions of nanoparticles in LCs have been shown to have substantial consequences, directly affecting the character of phase transitions. Characteristically for the *I*-*N* transition, it has been demonstrated that the onset of the nematic order, upon cooling from the *I* phase, follows a two-step process (doubling of the transition), from a random-dilution regime to a random-field, low-temperature regime [21]. Extensive studies of the *N*-Sm*A* transition of the thermotropic liquid crystal 4-n-pentylphenylthiol-4-n-octyloxybenzoate ($\bar{8}$S5) reveal that the critical character remains unaffected by the aerosil-introduced quenched-random disorder. Even though the *N*-Sm*A* is a pseudotransition, due to the destruction of the quasilong-range smectic order, the critical exponents derived from high-resolution heat-capacity data remain three-dimensional *XY*-like, for a large range of nanoparticle concentrations included in the study [22]. In addition, investigating the effects of aerosils upon the smectic order of aligned and nonaligned gels of octylcyanobiphenyl

*nounesis@rrp.demokritos.gr

(8CB), it was demonstrated that quenched randomness in aligned gels leads to constant three-dimensional XY critical exponents while otherwise a random field with disorder strength linearly dependent upon the nanoparticle concentration must be considered [9,23–25].

For the SmA-SmC transition of $\bar{8}$S5, the systematic analysis of high-quality calorimetric data has provided evidence for a tricritical to classical mean-field behavior of the heat-capacity peaks as well as for a substantial decrease of the heat-capacity jump as a function of aerosil concentration [22]. On the other hand, high-resolution x-ray diffraction experiments measuring the temperature dependence of the order parameter revealed nanoparticle-induced extensive coexistence regions and smearing of the data near the transition temperature [26]. When the aerosils are dispersed in the ferroelectric liquid crystal CE8, the effects upon SmA-SmC^* transition are even more severe. The strong coupling of hydrophilic aerosils with the liquid crystal establishes a pretransitional compression of the smectic layers extended well into the SmA phase while smearing effects are recorded near the transition for the temperature dependence of the order parameter, the dielectric constant, and the heat capacity, indicative of a crossover to supercritical-like transformations [14,15,27,28].

While aerosils dispersed in pentylcyanobiphenyl (5CB) have been shown to form agglomerates randomly [29], a new family of nanoparticles has recently been introduced, exhibiting a great capability for homogeneous dispersions in liquid-crystal hosts. These are spherical CdSe quantum dots surface-treated with oleylamine (OA) and trioctyl phosphine (TOP) that can be produced essentially monodisperse, with a core diameter $d \sim 3.5$ nm. These nanoparticles have demonstrated their capacity of altering the inherent bulk properties of their hosts. They can stabilize Blue Phase III (BPIII) for temperature ranges that are wider even by a tenfold from the bulk [30–32]. This property can be understood on the basis of a partial defect-core replacement mechanism [30,32], analogous to polymer-stabilization [33], that is coming to play due to the interactions of the CdSe quantum dots with disclination lines. Most recently, the same nanoparticles have also been shown to induce a twist grain boundary phase, by an analogous mechanism targeting screw dislocations. These results outline the great potential of the surface-functionalization moieties such as OA to adaptively interact with the cores of topological defects [34].

In this paper, we explore the effects from dispersing OA + TOP-treated CdSe nanoparticles in the SmA phase of the liquid-crystal compound CE8. In addition, we investigate the SmA-SmC^* phase transition by employing high-resolution ac calorimetry and x-ray scattering. We show that, contrary to aerosils, the CdSe quantum dots can increase the smectic layer periodicity, indicating a tendency of the nanoparticles to accumulate at the smectic layers, where the orientational and translational disorder are enhanced. Moreover, for the SmA-SmC^* transition, we show that calorimetric anomalies display an evolution to a step-like shape as the nanoparticle concentration is increased. This might be the signature of a crossover from near-tricritical to classical mean-field-like character of the transition. It would thus appear that the excessive accumulation of nanoparticles and the increase of the smectic layer thickness, is probably affecting the coupling between SmA and SmC^* order parameters that is responsible for the near-tricritical-point behavior observed in bulk samples. The effects of the nanoparticle dispersion upon the transition from SmC^* to tilted hexatic phases and hexatic-hexatic transitions are also discussed.

II. EXPERIMENTAL PROCEDURES

For all the experiments reported in this manuscript, the liquid crystal CE8 was supplied by Merck and was used without any additional treatment. The surface-treated CdSe quantum have been synthesized in N.C.S.R. "Demokritos." They are essentially monodisperse and have an average diameter of 3.5 nm [35]. They are highly soluble in nonpolar solvents such as hexane, toluene, and chloroform. Details on the preparation and the characterization of the CdSe nanoparticles have been described elsewhere [30,32].

The nanoparticles were dispersed in CE8 by mixing solutions of both components in a common solvent of high-purity (toluene). The resulting solution was sonicated for at least 5 min and then stirred at $\sim$85°C for several hours, as long as the solvent was evaporated by a steady stream over the open glass vials. Thereafter, all mixtures were dried under vacuum for 24 h. The uniform distribution of the nanoparticles in the LC samples has been consequently checked using optical and fluorescence microscopy [32]. In the low-temperature phases, the reproducibility of the calorimetric results for consecutive heating and cooling scans provides evidence that no further phase separation has taken place. For reasons of consistency with other reports of LC+nanoparticle mixtures [30–32,34] and in order to define the quantum dot concentration in the LC dispersion, the temperature-independent parameter $\chi = m_{np}/(m_{np} + m_{lc})$ has been used. Samples of various concentrations have been prepared: $\chi = 0.02$, 0.07, and 0.20.

For the x-ray measurements, samples with the exact same nanoparticle concentrations were placed in thin tubes (Hilgenberg-Mark tubes of 1-mm inner diameter) and were then attached to a computer-controlled heating stage by Instec Inc., with a temperature stability of $\pm$ 0.01 K. Measurements were taken at selected temperatures in the SmA, the SmC^*, and the hexatic phases. The x-ray setup consists of a Rigaku RUH-3R rotating anode generator, operating at 5.4 KW and producing a beam of $\lambda = 1.5416$ Å (K_a line of Cu). A flat graphite was used as a monochromator. Point focusing of the beam (0.3×0.3 mm^2) was attained by double focusing mirrors by Molecular Structure Corp., in a continuous He flow. The detector was an R-Axis IV double imaging plate system (area of 300×300 mm^2) built by Molecular Structure Corp. The pixel size was 100×100 μm^2 and the sample-to-detector distance during experiments was set to 279 mm. The dynamic range of this system is 10^6 and the resolution is 0.004 Å^{-1} (half-width at half-maximum).

The heat-capacity data for CE8 and its mixtures with the CdSe nanoparticles have been obtained using a fully computerized, high-resolution ac calorimeter. The calorimeter is capable of operating in the ac mode as well as in the so-called relaxation or nonadiabatic scanning mode. The ac mode is sensitive only to continuous enthalpy changes, while the phase of the ac temperature oscillations can indicate whether a transition is first or second order. The relaxation

mode on the other hand is sensitive to both continuous and discontinuous (latent heat) enthalpy changes. The comparison of the data between the two modes of operation can provide a quantitative determination of the released latent heat. A detailed description of the apparatus, the modes of operation, and its usefulness in studies of phase transitions and critical phenomena can be found in Refs. [36–38]. Sample quantities of 40 mg were placed in silver cells and mounted in the calorimeter. Afterwards they were heated to the I phase and slowly cooled along the various mesophases. The heat capacity of the empty cell was subtracted and the result was divided by the sample mass in order to obtain the net specific heat capacity (C_p) of the samples.

III. RESULTS AND DISCUSSION

The temperature versus nanoparticle concentration (T-χ) phase diagram for CE8 and mixtures containing dispersed CdSe nanoparticles surface-treated with OA and TOP has been thoroughly investigated by high-resolution ac calorimetry as well as optical microscopy. The area of the phase diagram that includes the SmA-SmC^*-hexatic phase transition lines is illustrated in Fig. 1. It is characterized by a steep downward shift of the SmA-SmC^* transition temperature even for the smallest concentration of quantum dots. The SmC^* temperature range shrinks to 7.3 K for the $\chi = 0.02$ sample and to 3.2 K for the $\chi = 0.20$ one with respect to 17.1 K for bulk CE8. On the other hand, the transition lines of the smectic-hexatic and hexatic-hexatic phase transitions are relatively stable exhibiting only small (∼2 K) downshifts.

The full data sets for calorimetric measurements of the $\chi = 0.02$, 0.07, and 0.20 mixtures are presented in Fig. 2 for a 40-degree temperature range (∼325 to 365 K). These

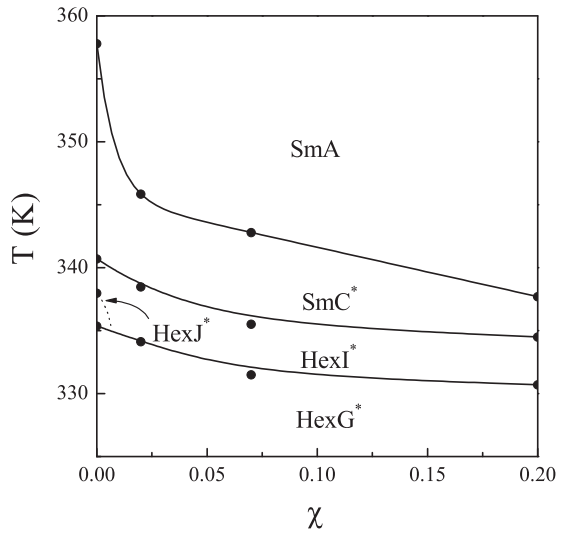

FIG. 1. T-χ phase diagram of CE8 containing dispersed CdSe nanoparticles in the area where SmA and SmC^* and hexatic phases exist. The symbols indicate measurements obtained using high-resolution ac calorimetry, cooling runs only, while the solid lines serve as guides to the eye. The distinction between the various hexatic phases is based upon previously published reports as well as on optical microscopy measurements obtained in the present study.

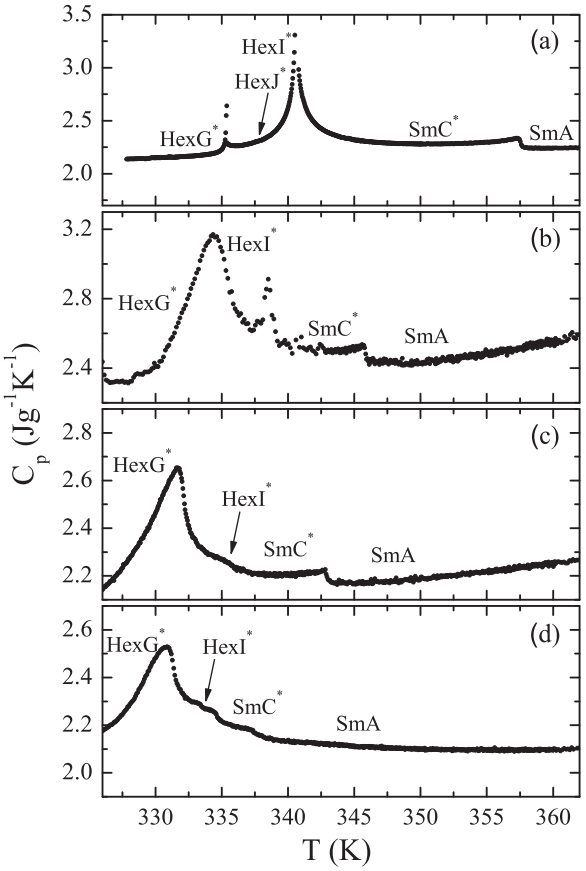

FIG. 2. C_p vs. T profiles obtained by ac mode of operation upon cooling through the smectic and hexatic phases of CE8 (a) and mixtures containing $\chi = 0.02$ (b), 0.07 (c), and 0.20 (d) CdSe nanoparticles.

are all cooling runs that commenced in the isotropic phase. For all the experiments, the cooling rate used is 0.3 Kh^{-1}. It is straightforwardly depicted that the SmA-SmC^* transition temperature of bulk CE8 drifts to lower temperatures (∼15 K) as the nanoparticle concentration is increased. In addition, dramatic changes take place concerning the shape of the C_p peaks of the smectic-hexatic and hexatic-hexatic phase transitions. The SmC^*-HexI^* peak evolves as a function of χ to an enthalpically weak anomaly, which remains relatively sharp for the $\chi = 0.02$ mixture, becoming dramatically suppressed with a virtually disappearing trace for the $\chi = 0.07$ and 0.20 samples. On the other hand, the HexI^*-HexG^* peak becomes progressively smeared and rounded with increasing χ rendering it impossible to distinguish the peak for the HexI^*-HexJ^* transition occurring on its high-T wing. This peak is characterized by a small enthalpic content even in the case of bulk CE8. In a sense, the broadened calorimetric peak can be viewed as the result of the merging of the SmC^*-HexI^*-HexJ^*-HexG^* transitions. In the phase diagram this merging is represented by the abolishment of the HexJ^* phase even for the lowest measured χ.

X-ray diffraction measurements have been carried out in order to monitor the effects of nanoparticles upon the smectic layer periodicity. Powder scattering profiles have been collected at various temperatures in the SmA phase for bulk CE8. Within the low-resolution limits of our experimental set

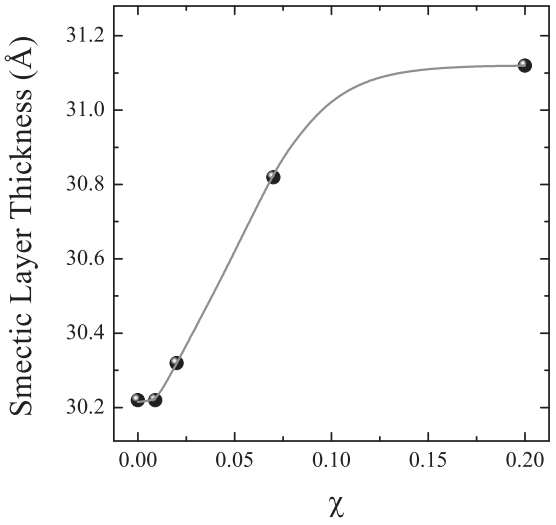

FIG. 3. Smectic layer thickness vs. χ well in the SmA phase, away from the SmA-SmC^* phase transition. The solid line serves as a guide to the eye.

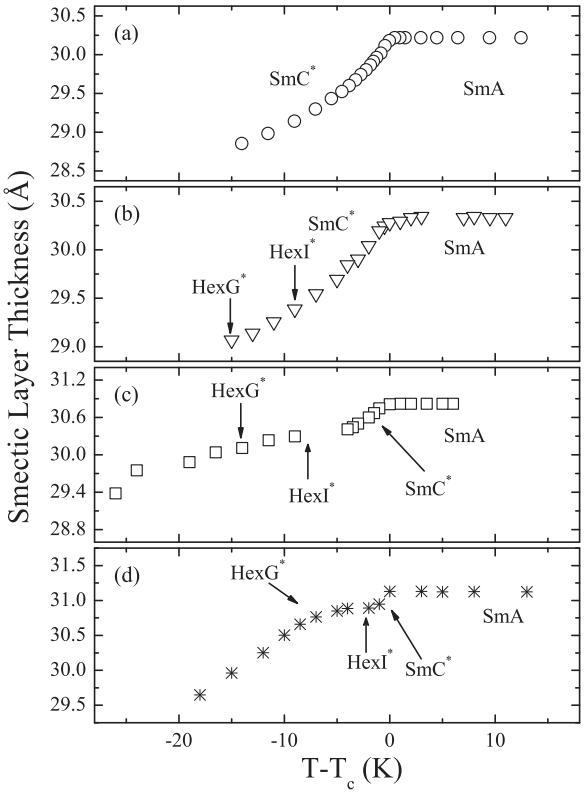

FIG. 4. Smectic layer thickness vs. T-T_c (where T_c is the SmA-SmC^* transition temperature) for cooling from the SmA to the HexG^* phase: (a) bulk CE8, (b) $\chi = 0.02$ mixture, (c) $\chi = 0.07$, and (d) $\chi = 0.20$. The estimation of the phase ranges, marked by the arrows, has also been based on the calorimetric data presented in Fig. 2.

up, it is not possible to quantify the impact of the nanoparticle dispersion upon the smectic correlations. In general, in the SmA phase, the hybrid materials exhibit broader diffraction peaks than bulk CE8, but no specific trends as a function of χ can be observed. Analogous is the situation in the SmC^* phase, while at lower temperatures in the HexG^* phase the peaks become sharper with a ∼5–10% reduction in the full width at half maximum values. For each concentration of the CdSe dispersions we find that the smectic layer thickness in the SmA phase is temperature independent. On the other hand, the smectic periodicity itself is severely altered. As it can straightforwardly be observed from the measurements displayed in Fig. 3, the layer thickness is strongly dependent upon χ. It increases from 30.22 Å for bulk CE8 to 31.12 Å for the $\chi = 0.20$ sample in a nonlinear manner. While the overall change is small, it nevertheless demonstrates the capability of the surface-treated nanoparticles to continuously alter the length of the layer spacing.

Previous x-ray diffraction studies of the SmA phase of CE8 doped with aerosils have revealed substantially different results [14,15]. Contrary to the present study, a mild compression of the smectic layers was reported in the SmA phase that was associated to a global pretransitional tilt [20]. It is thus reasonable to assume that the nature of the presently investigated CdSe interactions with CE8 must be very different than for the aerosils. In the scattering experiment on the CE8 + aerosils mixtures, it was revealed that even the smallest concentration $\chi = 0.05$ of aerosils induced a substantial broadening of the scattering peaks providing evidence for a direct effect upon the smectic correlations. An analogous behavior was also found in a different high-resolution x-ray study of the nonchiral liquid crystal $\overline{8}$S5 containing aerosils where a detailed line-shape analysis of the $\overline{8}$S5 smectic structure factor in the SmA as well as in the SmC phase, for a wide range of aerosil concentrations [26], solidly established the broadening of the x-ray diffraction peaks as a function of aerosil concentration. In the microscopic scale, the reduction of the range of smectic correlations was attributed to the strong pinning of the ferroelectric CE8 molecules on the surfaces of the aerosils, as well as to finite-size effects due to the confinement of the liquid-crystal molecules in the cavities created by the random networking of the self-assembling aerosils in the high-χ dispersion regime.

Turning the focus on the SmA-SmC^* phase transition, the temperature dependence of the smectic layer thickness across the transition and to lower temperatures into the hexatic phases, is presented in Fig. 4. Large downward drifts of the SmA-SmC^* transition temperature have been observed as a function of χ comparable to the findings from ac calorimetry, although small deviations do occur from one technique to the other as a result of the different thermometry. The tilt-angle of the liquid-crystal long molecular axis (θ) with respect to the smectic-layer normal is the order parameter of the SmA-SmC^* transition. To calculate θ based on the smectic layer spacing in the SmA phase (d) and the SmC^* phase (d_C), the following relationship can be used: $\theta = \arccos(d/d_C)$. Based on this calculation, the tilt angle temperature dependence $\theta(T - T_c)$, where T_c is the SmA-SmC^* transition temperature, is displayed in Fig. 5 for bulk CE8 as well as for the three quantum-dot mixtures under investigation. It is apparent that all the $\theta(T - T_c)$ profiles of the mixtures show deviations from the behavior of the bulk. Characteristically, at temperatures just below T_c, the data for $\chi = 0.02$ mixture indicate irregularities that may be likely linked to nanoparticle-induced phase coexistence regions, as was the case in the $\overline{8}$S5 + aerosil

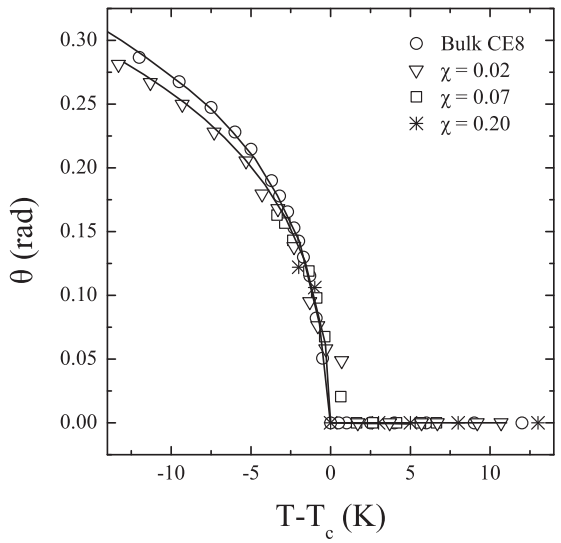

FIG. 5. Tilt angle (θ) vs. T-T_C for bulk CE8 and the three mixtures with CdSe nanoparticles. As in all the other figures, open circles correspond to bulk CE8, triangles to the $\chi = 0.02$, squares to the $\chi = 0.07$, and asterisks to the $\chi = 0.20$ mixture. The solid lines are fits of the data using the EMF model [Eq. (2)].

system. At even lower T, in the SmC^* phase, the tilt angle for the $\chi = 0.02$ and 0.07 samples cannot fully reach the values exhibited by bulk CE8.

The SmA-SmC^* transition has been successfully analyzed by an extended-mean-field model (EMF) [39]. The EMF model can be described by Eq. (1):

$$\theta = \left(\frac{b}{3c}\right)\left[\left(1-\frac{3t}{t_o}\right)^{1/2}-1\right]^{1/2} \quad T < T_c$$
$$\theta = 0 \quad T > T_c. \tag{1}$$

Here, $t = (T_c - T/T_c)$ and $t_o = b^2/ac$ distinguishes between mean-field (MF) and EMF-type of behavior. The latter is realized for $t_o \ll 1$. The parameters a, b, and c are the coefficients for the second-, fourth-, and sixth-order terms, respectively, in the Landau free-energy expansion in terms of θ [39]. The solid lines illustrated in Fig. 5 are nonlinear, least-squares fits of the data for bulk CE8 and the $\chi = 0.02$ mixture to the EMF model [Eq. (1)] with the set of parameters given below: $R = b/3c = 0.031$ and $t_o = 0.0073$ for bulk CE8 and $R = 0.042$ and $t_o = 0.015$. For the $\chi = 0.02$ mixture, the points nearest T_c have been omitted from the fit.

So far, aerosil dispersions of $\bar{8}$S5 have been shown to fundamentally alter the character of the SmA-SmC transition by limiting the range of the smectic correlations and by inducing, among others, extended phase coexistence regions as a result of the quenched-random field disorder. A similar situation is depicted for the SmA-SmC^* transition of aerosil mixtures with CE8. In this case, extensive pretransitional tilted order in the SmA phase has been also recorded, manifested as a compression of the smectic layers, even at 10 K away from the transition temperature. Moreover, the smearing of the $\theta(T)$ profiles was observed as a function of increasing aerosil concentration to an almost linear T-dependence for the $\chi = 0.15$ mixture, as well as a substantial reduction to the tilt-angle values and downshifts of T_c, demonstrating dramatic deviations from the EMF model, into the regime of smeared, supercritical-like transformations. As it was mentioned previously, the observed irregular behavior of the order parameter is attributed to the particularly strong quenched-random-disorder field in the SmC or SmC^* phases due the pinning of the chiral liquid-crystal molecules on the surface of the aerosils. Comparisons with the results for the present system highlight two main, substantial differences: In the case of the CdSe nanoparticles, the SmA layer thickness increases with increasing χ and T_c exhibits extensive downshifts even for the smallest χ.

The increase of the length of the layer periodicity can be attributed to the tendency of the surface-treated nanoparticles to accumulate in the more structurally chaotic regions of their liquid-crystalline environment. This is why nanoparticles interact by partially replacing the cores of screw dislocations [40] as well as of edge dislocations in the smectic layers [41,42]. Recently, it has been shown that a mechanism based on the adaptive-defect-core-targeting (ADCT) of disclination lines and screw dislocations can stabilize BPIII as well as a twist-grain-boundary-A phase (TGB$_A$), at temperatures between the N^* and the SmA phases [31,32,34]. For spherical nanoparticles of appropriate size, the adaptability has been shown to depend upon the flexibility of the functionalizing moieties on their surface, such us OA [34]. For the nanoparticles to substantially increase the smectic layer periodicity, though, their accumulation at the smectic layers must certainly exceed the regions of defect cores.

Turning to a detailed analysis of the C_p results, Fig. 6 displays the excess heat capacity (ΔC_p) for bulk CE8 and the three CdSe nanoparticle mixtures. No phase-coexistence region has been detected for any of the three mixtures, indicating that the nanoparticle dispersion bears only minimum effects upon the character of the SmA-SmC^* phase transition. Moreover, no thermal hysteresis has been recorded when performing consecutive heating and cooling cycles. On the other hand, large downshifts of the transition temperature

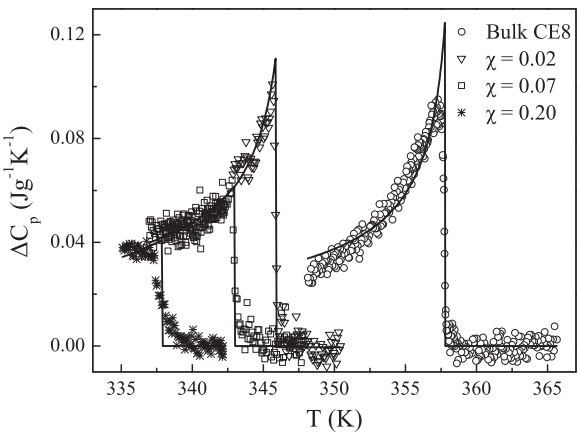

FIG. 6. Excess heat capacity ΔC_p vs. T profiles for the SmA-SmC^* transition peaks of bulk CE8 and three mixtures containing $\chi = 0.02$, 0.07 and 0.20 dispersed quantum dots. All the data are obtained on ac mode upon cooling the samples. The solid lines are fits to the EMF model presented in the text [Eq. (2)].

TABLE I. Parameters obtained from nonlinear least-squares fits of the EMF model [Eq. (2)] to the excess heat-capacity data $\Delta C_p(T)$ presented in Fig. 6.

	A ($\mathrm{Jg^{-1}K^{-1}}$)	T_c (K)	T_m (K)
Bulk CE8	0.125 ± 0.002	357.78	358.72 ± 0.06
$\chi = 0.02$	0.114 ± 0.003	345.92	347.19 ± 0.16
$\chi = 0.07$	0.060 ± 0.003	343.02	347.54 ± 0.24
$\chi = 0.20$	0.040 ± 0.003	337.90	344.91 ± 0.87

are recorded. In addition, a reduction in the size of the heat-capacity peak is evidenced along with a crossover of its shape to a step-like anomaly for the $\chi = 0.20$ mixture. While the T_c drifts have not been observed in the case of $\overline{8}$S5 + aerosil mixtures [11], they have been recorded in the case of calorimetric measurements of 7O.4 + aerosils [43]. The evolution of the ΔC_p shape to step-like for the $\chi = 0.20$ sample, however, is in line with what has been reported for the $\overline{8}$S5 + aerosil mixtures [22]. On the contrary, the CE8 + aerosils mixtures exhibited a substantially different behavior where, analogously to the tilt angle, the heat-capacity profiles evolved into broadened and smeared supercritical anomalies as a function of increasing χ, with a rapidly decreasing enthalpic content.

After the subtraction of the appropriate background contribution, the heat-capacity peaks displayed in Fig. 6 have been analyzed using the EMF model of Eq. (2) [39]:

$$\begin{aligned} \Delta C_p &= A\frac{T}{T_c}\left(\frac{T_m - T_c}{T_m - T}\right)^{1/2} \quad T < T_c \\ \Delta C_p &= 0 \quad T > T_c, \end{aligned} \tag{2}$$

Here the heat-capacity jump is defined as $A = a^2/2bT_c$, and $T_m = (t_o/3 + 1)T_c$ provides a measure of the proximity to the tricritical point. The parameter t_o has been defined before, while a, b are defined in the expansion of the Landau free energy. Fitting of the ΔC_p data to Eq. (2) produces the results presented in Table I. It is straightforwardly evidenced that besides the reduction of the heat-capacity jump A, an EMF to MF crossover is observed for the shape of the heat-capacity anomaly. In the previous study by Roshi *et al.* [22], a relation of the form $A \sim \rho_s^{-0.5}$ was shown to hold, characteristic of the EMF to MF crossover, where ρ_s is the density of aerosils. An analogous expression is also found to describe the present data with an exponent of 0.49 ± 0.02.

The observed ΔC_p crossover behavior can be interpreted in the context of the dispersed CdSe nanoparticles driving the SmA-SmC^* transition of CE8 away from tricriticality toward a more step-like, mean-field behavior. The proximity of the transition to a tricritical point is mainly depended upon the elastic constant B via the coupling of the tilt-order parameter and the layer compression [44]. An analogous crossover effect could not be established by our x-ray diffraction results. This must be attributed to the scarcity of the scattering data points near T_c and the very few data points available in the SmC^* phase for the $\chi = 0.07$ and 0.20 samples, which makes it impossible to discern between MF and EMF behavior. It can be argued, though, that the trend toward MF-like behavior and the decreasing size of the ΔC_p step are indicative of the hardening of B [22]. For the present data, the local accumulation of the nanoparticles at the smectic layers can substantially contribute to the hardening of the layer elasticity. Moreover, the increase of the layer thickness may weaken the coupling of the SmA and SmC^* order parameters responsible for giving to the bulk transition its tricritical character.

In the case of the smectic-hexatic transitions, the dispersion of the OA + TOP-treated CdSe nanoparticles in CE8 affects the character of the transitions far more severely. This of course is depicted by the x-ray as well as the calorimetric results. Within the temperature range of the HexI^* phase, the smectic layer thickness for the $\chi = 0.07$ and $\chi = 0.20$ mixtures, as it can be seen in Figs. 4(c) and 4(d), remains relatively constant. This is a surprising behavior for a tilted hexatic phase occurring only a few degrees below the SmA-SmC^* transition. For hexatic phases of a narrow temperature width, it is generally expected that the tilt-angle values would continue to increase in the HexI^* phase as it is the case for the $\chi = 0.02$ mixture [Fig. 4(b)]. Moreover, the SmC^*-HexI^* transition calorimetric peak virtually disappears for the $\chi = 0.07$ and the $\chi = 0.20$ samples, while for $\chi = 0.02$ it retains the characteristic sharp shape of the bulk compound, albeit with substantially smaller enthalpic signal sensed by the ac operational mode of the calorimeter. For LC compounds as well as for LC binary mixtures, the character of the smectic-hexatic phase transitions is substantially affected by the coupling between the smectic and the hexatic order parameters. This has been demonstrated by x-ray as well as by calorimetric results for systems in the vicinity of a smectic-hexatic-crystal triple point [45,46]. The evolution of the calorimetric peaks observed here is likely reflecting the crucial role of the CdSe nanoparticles in the weakening of the smectic-hexatic coupling by increasing the smectic layer periodicity and/or destroying the long-range bond-orientational order. On the other hand, the shape of HexI^*-HexG^* calorimetric anomaly may reflect the merge of the various hexatic-hexatic transition peaks. It is interesting to note that the molecular tilt, which was stable in the temperature range of HexI^* phase, is increasing again in the HexG^* phase as a function of temperature as demonstrated by the compression of the smectic layers as depicted in Figs. 4(c) and 4(d).

IV. CONCLUSIONS

The structural and calorimetric results presented here demonstrate that OA and TOP surface-treated CdSe nanoparticles can locally accumulate at the smectic layers, increasing the length of the smectic layer periodicity of CE8. The targeting of the smectic layers is most probably based on the tendency of OA and TOP surface-treated nanoparticles to accumulate in the more organizationally disordered regions of the liquid-crystalline medium. This has already been shown to be the case for the cores of disclination lines in blue phases [32] and screw dislocations in a TGB$_A$ phase [34]. In phases with quasilong-range smectic order, the targeting may also include edge dislocations. The increase of the layer thickness as well as a possible nanoparticle-induced hardening of their elasticity can weaken the coupling of the

SmA and SmC^* order parameters. This leads to an apparent near-tricritical mean-field to classical mean-field crossover of the character of the SmA-SmC^* transition. Moreover, the dispersion of the surface-functionalized nanoparticles seriously disrupts the smectic-hexatic phase sequence of the bulk CE8.

It thus appears that the OA- and TOP-treated CdSe quantum dots interact adaptively with chiral LCs, such as CE8, providing opportunities for affecting LC properties in ways that can lead to diverse technological applications. In this direction, more systematic work must be planned involving spherical nanoparticles with diameters between 3 and 4 nm, functionalized with LC-compatible hydrophobic moieties that display the spatial and orientational flexibility of OA.

ACKNOWLEDGMENTS

This work has been supported in part by a grant from the J. S. Latsis Public Benefit Foundation. E.K. acknowledges the support of the Graduate Fellowship Program of N.C.S.R. "Demokritos." G.C. and V.T. acknowledge the financial support by the Project No. PE3-1535 implemented within the framework of the Action "Supporting Postdoctoral Researchers" of the Operational Project "Education and Lifelong Learning," cofinanced by the European Social Fund and the Greek State. Z.K. acknowledges the support by the Program No. P1-0125 of the Slovenian Research Agency. The use of the x-ray diffraction facilities of the Center for Crystallography of Macromolecules of N.C.S.R. "Demokritos" is greatly appreciated.

[1] T. Hegmann, H. Qi, and V. M. Marx, J. Inorg. Organomet. Polym. Mater. **17**, 483 (2007).
[2] M. Draper, J. M. Saez, S. J. Cowling, P. Gai, B. Heinrich, B. Donnio, D. Guillon, and J. W. Goodby, Adv. Funct. Mater. **21**, 1260 (2011), and references therein.
[3] H. Qi and T. Hegmann, J. Mater. Chem. **18**, 3288 (2008).
[4] D. Coursault, J. Grand, B. Zappone, H. Ayeb, G. Levi, N. Félidj, and E. Lacaze, Adv. Mater. **24**, 1461 (2012).
[5] J. W. Taylor, L. K. Kurihara, and L. J. Martinez-Miranda, Appl. Phys. Lett. **100**, 173115 (2012).
[6] A. R. Hirst, B. Escuder, J. F. Miravet, and D. K. Smith, Angew. Chem. Int. Ed. **47**, 8002 (2008).
[7] G. S. Iannacchione, C. W. Garland, J. T. Mang, and T. P. Rieker, Phys. Rev. E **58**, 5966 (1998).
[8] M. Marinelli, A. K. Ghosh, and F. Mercuri, Phys. Rev. E **63**, 061713 (2001).
[9] R. L. Leheny, S. Park, R. J. Birgeneau, J. L. Gallani, C. W. Garland, and G. S. Iannacchione, Phys. Rev. E **67**, 011708 (2003).
[10] G. S. Iannacchione, S. Park, C. W. Garland, R. J. Birgeneau, and R. L. Leheny, Phys. Rev. E **67**, 011709 (2003).
[11] P. S. Clegg, C. Stock, R. J. Birgeneau, C. W. Garland, A. Roshi, and G. S. Iannacchione, Phys. Rev. E **67**, 021703 (2003).
[12] S. Frunza, L. Frunza, M. Tintaru, I. Enache, T. Beica, and A. Schonhals, Liq. Cryst. **31**, 913 (2004).
[13] T. Jin and D. Finotello, Phys. Rev. Lett. **86**, 818 (2001).
[14] G. Cordoyiannis, G. Nounesis, V. Bobnar, S. Kralj, and Z. Kutnjak, Phys. Rev. Lett. **94**, 027801 (2005).
[15] G. Cordoyiannis, S. Kralj, G. Nounesis, Z. Kutnjak, and S. Žumer, Phys. Rev. E **75**, 021702 (2007).
[16] M. Ramazanoglu, S. Larochelle, C. W. Garland, and R. J. Birgeneau, Phys. Rev. E **77**, 031702 (2008).
[17] J. Leys, C. Glorieux, and J. Thoen, J. Phys.: Condens. Matter **20**, 244111 (2008).
[18] J. Milette, C. T. Yim, and L. Reven, J. Phys. Chem. B **112**, 3322 (2008).
[19] U. Zammit, M. Marinelli, F. Mercuri, and S. Paoloni, J. Chem. Phys. B **113**, 14315 (2009).
[20] G. Cordoyiannis, S. Kralj, G. Nounesis, S. Žumer, and Z. Kutnjak, Phys. Rev. E **73**, 031707 (2006).
[21] M. Caggioni, A. Roshi, S. Barjami, F. Mantegazza, G. S. Iannacchione, and T. Bellini, Phys. Rev. Lett. **93**, 127801 (2004).
[22] A. Roshi, G. S. Iannacchione, P. S. Clegg, R. J. Birgeneau, and M. E. Neubert, Phys. Rev. E **72**, 051716 (2005).
[23] D. Liang, M. A. Borthwick, and R. L. Leheny, J. Phys.: Condens. Matter **16**, S1989 (2004).
[24] D. Liang and R. L. Leheny, Phys. Rev. E **75**, 031705 (2007).
[25] F. Cruceanu, D. Liang, R. L. Leheny, C. W. Garland, and G. S. Iannacchione, Phys. Rev. E **79**, 011710 (2009).
[26] B. Freelon, M. Ramazanoglu, P. J. Chung, R. N. Page, Y.-T. Lo, P. Valdivia, C. W. Garland, and R. J. Birgeneau, Phys. Rev. E **84**, 031705 (2011).
[27] Z. Kutnjak, S. Kralj, and S. Žumer, Phys. Rev. E **66**, 041702 (2002).
[28] Z. Kutnjak, G. Cordoyiannis, and G. Nounesis, Ferroelectrics **294**, 105 (2003).
[29] D. D. van't Zand, Y. Chushkin, L. Belkoura, C. V. Lobo, R. Strey, K. Lyakova, and P. S. Clegg, Soft Matt. **8**, 4062 (2012).
[30] E. Karatairi, B. Rožič, Z. Kutnjak, V. Tzitzios, G. Nounesis, G. Cordoyiannis, J. Thoen, C. Glorieux, and S. Kralj, Phys. Rev. E **81**, 041703 (2010).
[31] G. Cordoyiannis *et al.*, Liq. Cryst. **37**, 1419 (2010).
[32] B. Rožič *et al.*, Eur. Phys. J. E **34**, 17 (2011).
[33] H. Kikuchi, M. Yokota, Y. Hisakado, H. Yang, and T. Kajiyama, Nat. Mater. **1**, 64 (2002).
[34] G. Cordoyiannis *et al.*, Soft Matt. **9**, 3956 (2013).
[35] V. Tzitzios, V. Georgakilas, I. Zafiropoulou, N. Boukos, G. Basina, D. Niarchos, and D. Petridis, J. Nanosci. Nanotechno. **8**, 3117 (2008).
[36] H. Yao, K. Ema, and C. W. Garland, Rev. Sci. Instrum. **69**, 172 (1998).
[37] Z. Kutnjak, S. Kralj, G. Lahajnar, and S. Žumer, Phys. Rev. E **68**, 021705 (2003).
[38] Z. Kutnjak, J. Petzelt, and R. Blinc, Nature (London) **441**, 956 (2006).
[39] S. Dumrongrattana, G. Nounesis, and C. C. Huang, Phys. Rev. A **33**, 2181 (1986).
[40] I. Lelidis, C. Blanc, and M. Kleman, Phys. Rev. E **74**, 051710 (2006).
[41] R. B. Meyer, B. Stebler, and S. T. Lagerwall, Phys. Rev. Lett. **41**, 1393 (1978).

[42] I. Lelidis, M. Kleman, and J. L. Martin, Mol. Cryst. Liq. Cryst. **351**, 187 (2000).
[43] H. Haga and C. W. Garland, Phys. Rev. E **56**, 3044 (1997).
[44] P. de Gennes and J. Prost, *The Physics of Liquid Crystals* (Oxford University Press, Oxford, 1993).
[45] C. C. Huang, G. Nounesis, and D. Guillon, Phys. Rev. A **33**, 2602 (1986).
[46] D. J. Brock, A. Aharony, R. J. Birgeneau, K. W. Evans-Lutterodt, J. D. Litster, P. M. Horn, G. B. Stephenson, and A. R. Tajbakhsh, Phys. Rev. Lett. **57**, 98 (1986).